BOUNDARY-FITTED COORDINATE SYSTEMS FOR ARBITRARY COMPUTATIONAL REGIONS

Edward J. Kowalski
Boeing Military Airplane Company
Advanced Airplane Branch
Seattle, Washington 98124

A computational region of arbitrary cross section presents a significant problem in the generation of a mesh. Simple orthogonal meshes are difficult to use because the mesh points do not naturally fall on the region's boundaries. Differencing and interpolation schemes become complex and cumbersome, and it is difficult to extend these schemes to higher order because of the complex logic required. Higher order schemes are desirable as they allow calculation of a flow to a given level of accuracy with a lower mesh density and hence less storage than a lower order scheme. High accuracy solutions are possible for a region of arbitrary cross section when a boundary-fitted computational mesh is employed. A boundary-fitted mesh is defined as a mesh in which the boundary (i.e., a duct wall) is coincident with the mesh points that are used for finite difference expressions at, and adjacent to, the boundary. Interpolation is not required, and extension to higher order differencing is straightforward. This is a significant benefit when the boundary conditions have a dominant influence on the solution.

This paper will discuss the application of Smith and Wiegel's method for generating boundary fitted coordinate systems (discussed in their AIAA-80-0192 paper entitled, "Analytic and Approximate Boundary Fitted Coordinate Systems for Fluid Flow Simulation") for two practical flow problems characterized by complex surface geometry:

- o radial mixer lobe
- o subsonic inlet designed for high angle-of-attack capability

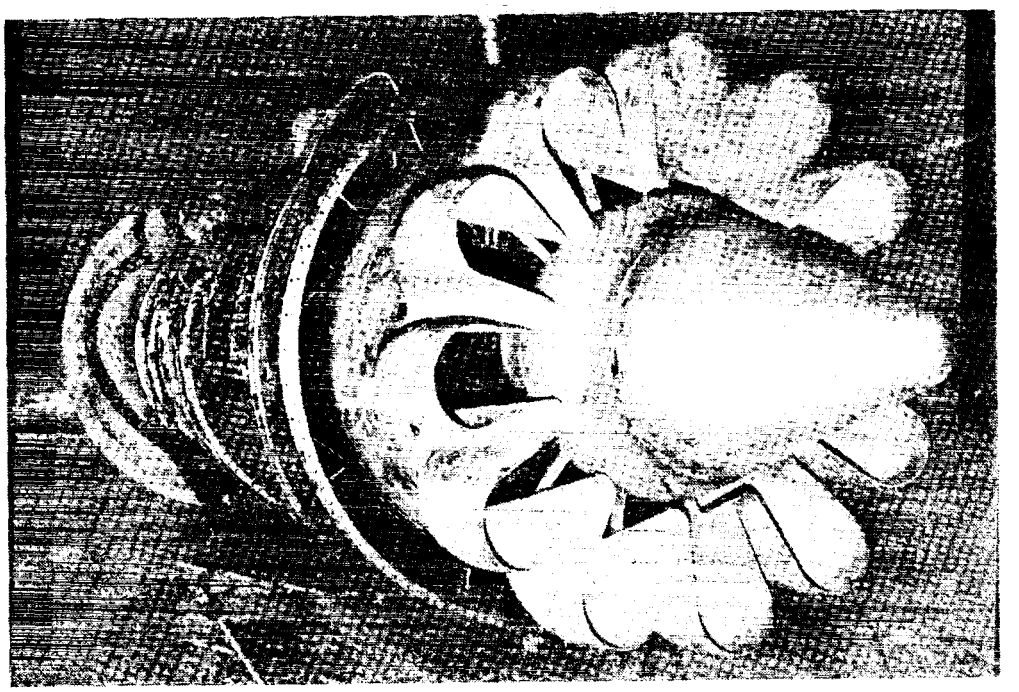

Figure 1.- Full scale forced mixer.

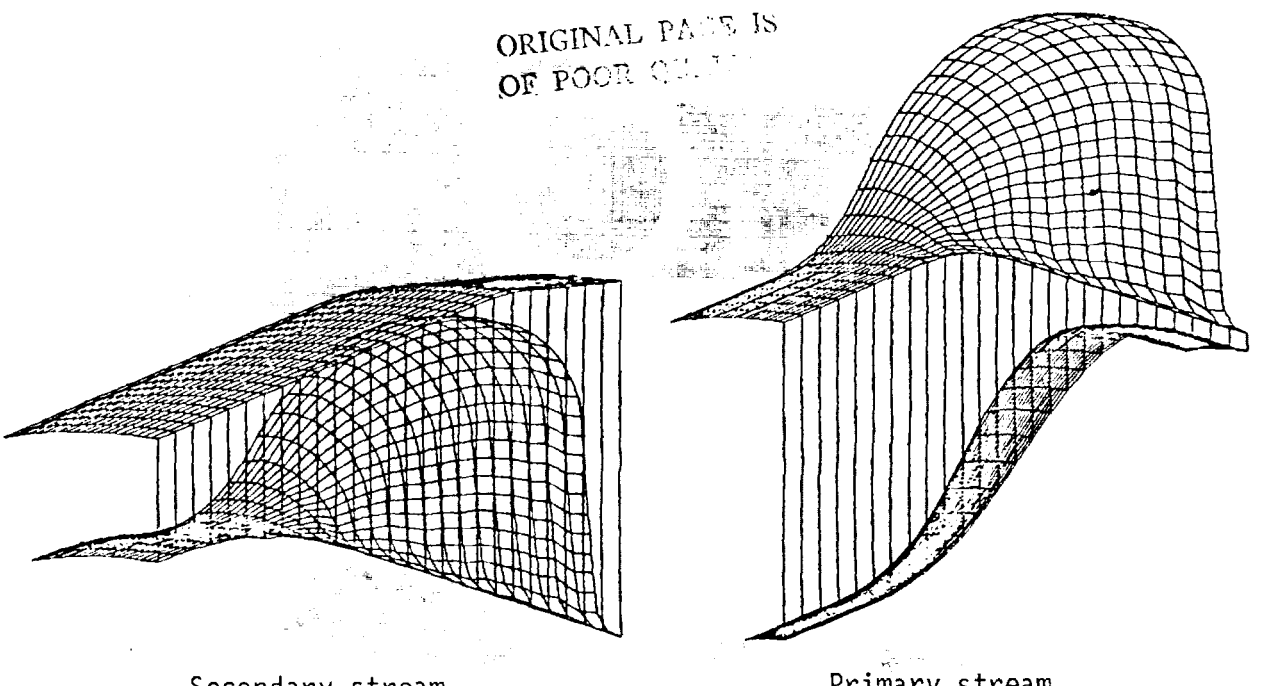

Figure 2.- Radial mixer lobe.

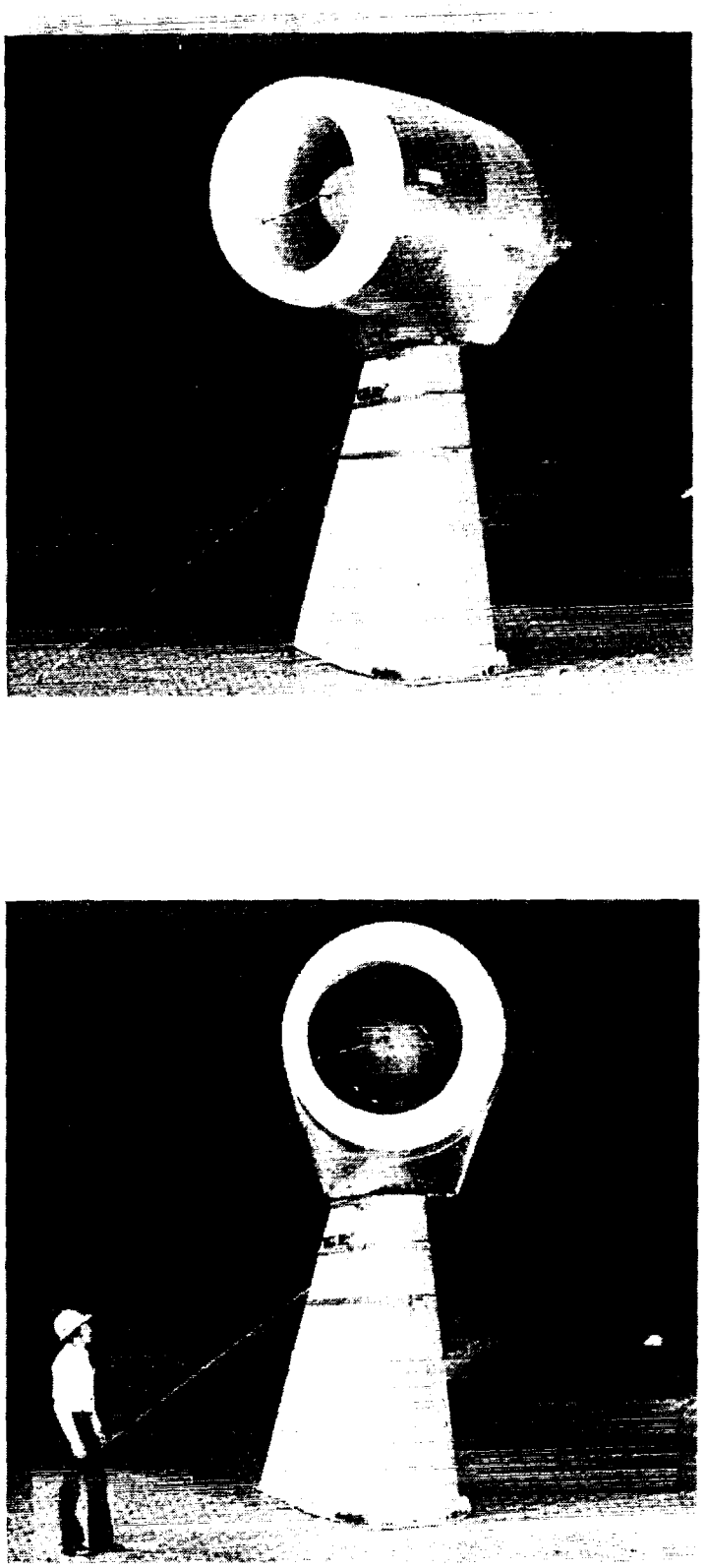

Figure 3.- Supersonic inlet.

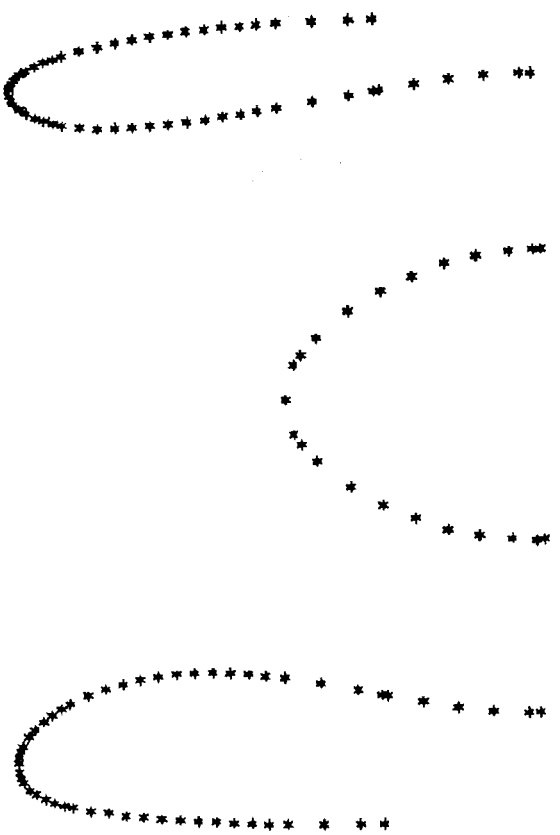

Figure 4.- Inlet contour.

In the method of Smith and Wiegel, two disconnected boundaries are defined and an explicit functional relation is used to establish the transformation between the physical domain and the computational domain.

The physical domain is defined by a cartesian coordinate system; the computational domain is defined with the variables ξ , η and ζ with the values:

$$0 \leq \xi \leq 1$$

$$0 \leq \eta \leq 1$$

$$0 \leq \zeta \leq 1$$

Two possible connecting functions are suggested: linear and a cubic parametric polynomial. The following cubic polynomial equation was used to generate meshes for both the lobe mixer and the subsonic inlet:

$$x = X_1(\xi,\zeta)f_1(\eta) + X_2(\xi,\zeta)f_2(\eta) + \frac{dX_1}{d\eta}(\xi,\zeta)f_3(\eta) + \frac{dX_2}{d\eta}(\xi,\zeta)f_4(\eta)$$

$$y = Y_1(\xi,\zeta)f_1(\eta) + Y_2(\xi,\zeta)f_2(\eta) + \frac{dY_1}{d\eta}(\xi,\zeta)f_3(\eta) + \frac{dY_2}{d\eta}(\xi,\zeta)f_4(\eta)$$

$$z = Z_1(\xi,\zeta)f_1(\eta) + Z_2(\xi,\zeta)f_2(\eta) + \frac{dZ_1}{d\eta}(\xi,\zeta)f_3(\eta) + \frac{dZ_2}{d\eta}(\xi,\zeta)f_4(\eta)$$

where:

$X_\ell(\xi,\eta), Y_\ell(\xi,\eta), Z_\ell(\xi,\eta), \ell = 1,2$ are the boundary points in the physical domain

$\frac{dX}{d\eta}_\ell(\xi,\eta), \frac{dY}{d\eta}_\ell(\xi,\eta) \frac{dZ}{d\eta}_\ell(\xi,\eta), \ell = 1,2$ are the derivatives of the boundary points in the physical domain

$$f_1(\eta) = 2\eta^3 - 3\eta^2 + 1$$
$$f_2(\eta) = -2\eta^3 + 3\eta^2$$
$$f_3(\eta) = \eta^3 - 2\eta^2 + \eta$$
$$f_4(\eta) = \eta^3 - \eta^2$$

The cubic connecting function forces orthogonality at the boundaries of the physical domain by calculating the derivatives $\frac{dX}{d\eta}_\ell(\xi,\eta)$ $\frac{dY}{d\eta}_\ell(\xi,\eta)$ and $\frac{dZ}{d\eta}_\ell(\xi,\eta)$ from the cross product of the tangential derivatives and then dividing by the magnitude of the normal vector.

Four extensions of the Smith and Wiegel method were necessary in order to successfully apply their technique to the mixer lobe and subsonic inlet.

First, because of the nature of the mixer and inlet geometries, points defining the boundaries had to be positioned using a geometric progression.

$$S = a + ar + ar^2 + \ldots + ar^{N-1}$$

$$= \frac{a(1-r^N)}{1-r}$$

where

S = the total length of the boundary

a = first increment

r = scale factor

N = number of cells (one less the number of boundary points)

For the mixer, the scale factor r was varied linearly from $r = 1$ at the mixer entrance plane (where the boundary is an arc) to $r = r_{max}$ at the mixer exit plane (where the boundary is highly distorted). This makes it possible to force the mesh to migrate to regions of interest without causing significant distortions in the mesh from plane to plane. The optimal distribution of mesh occurred when the upper and lower boundary mesh points were stretched in opposite directions.

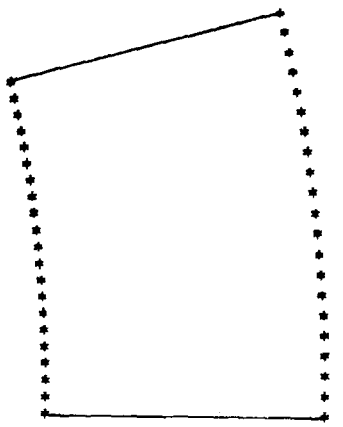

SECONDARY LOBE - PLANE 94
GEOMETRIC PROGRESSION LOWER BOUNDARY 1.0000 UPPER BOUNDARY 1.0000
SLOPE SCALER LOWER BOUNDARY 1.0000 UPPER BOUNDARY 1.0000

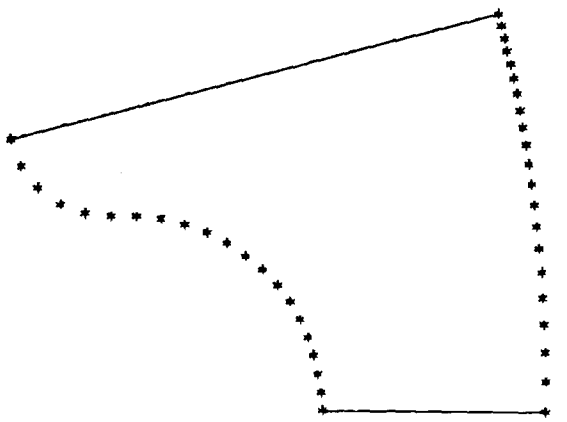

SECONDARY LOBE - PLANE 107
GEOMETRIC PROGRESSION LOWER BOUNDARY 0.9750 UPPER BOUNDARY 1.0500
SLOPE SCALER LOWER BOUNDARY 1.0250 UPPER BOUNDARY 1.0500

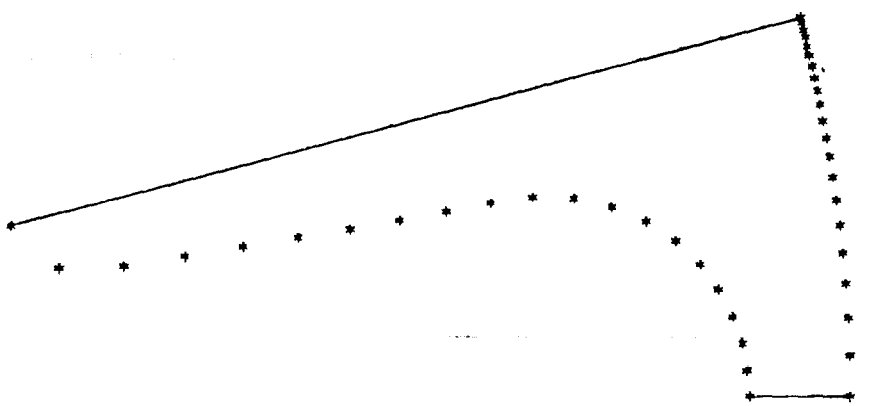

SECONDARY LOBE - PLANE 120
GEOMETRIC PROGRESSION LOWER BOUNDARY 0.9500 UPPER BOUNDARY 1.1000
SLOPE SCALER LOWER BOUNDARY 1.0500 UPPER BOUNDARY 1.1000

Figure 5.- Geometric progression for boundary points for secondary stream.

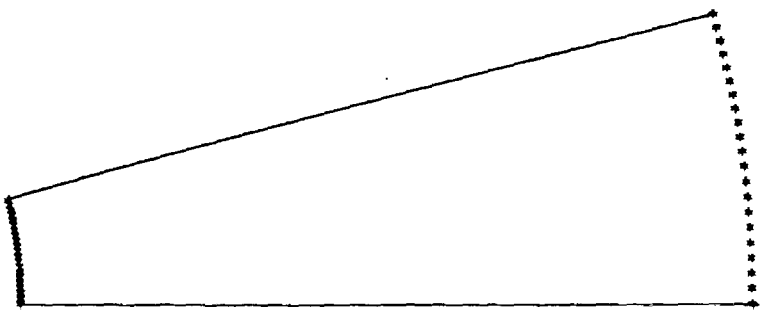

PRIMARY LOBE - PLANE 94
GEOMETRIC PROGRESSION LOWER BOUNDARY 1.0000 UPPER BOUNDARY 1.0000
SLOPE SCALER LOWER BOUNDARY 1.0000 UPPER BOUNDARY 1.0000

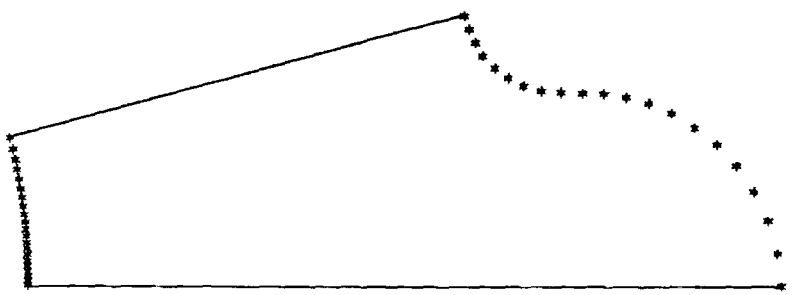

PRIMARY LOBE - PLANE 107
GEOMETRIC PROGRESSION LOWER BOUNDARY 1.0500 UPPER BOUNDARY 1.0500
SLOPE SCALER LOWER BOUNDARY 1.0500 UPPER BOUNDARY 1.0500

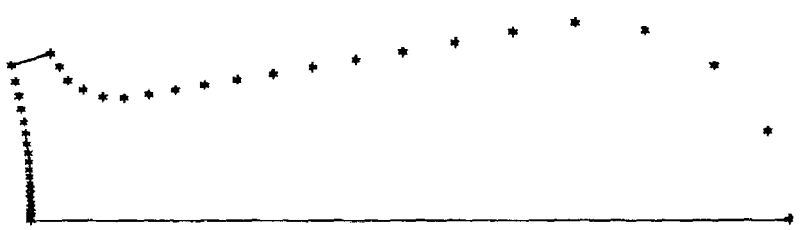

PRIMARY LOBE - PLANE 120
GEOMETRIC PROGRESSION LOWER BOUNDARY 1.1000 UPPER BOUNDARY 1.1000
SLOPE SCALER LOWER BOUNDARY 1.1000 UPPER BOUNDARY 1.1000

Figure 6.- Geometric progression of boundary points for primary stream.

The inlet has certain regions (hilite, throat, etc.) which require a fine computational mesh to insure a detailed analysis. For this reason, four regions along each inlet contour and five regions along the boundary of the analysis domain required individual geometric progressions. The scale factor, r, and the number of cells, N, of each region must be chosen to insure a smooth progression in cell length along each of the boundaries.

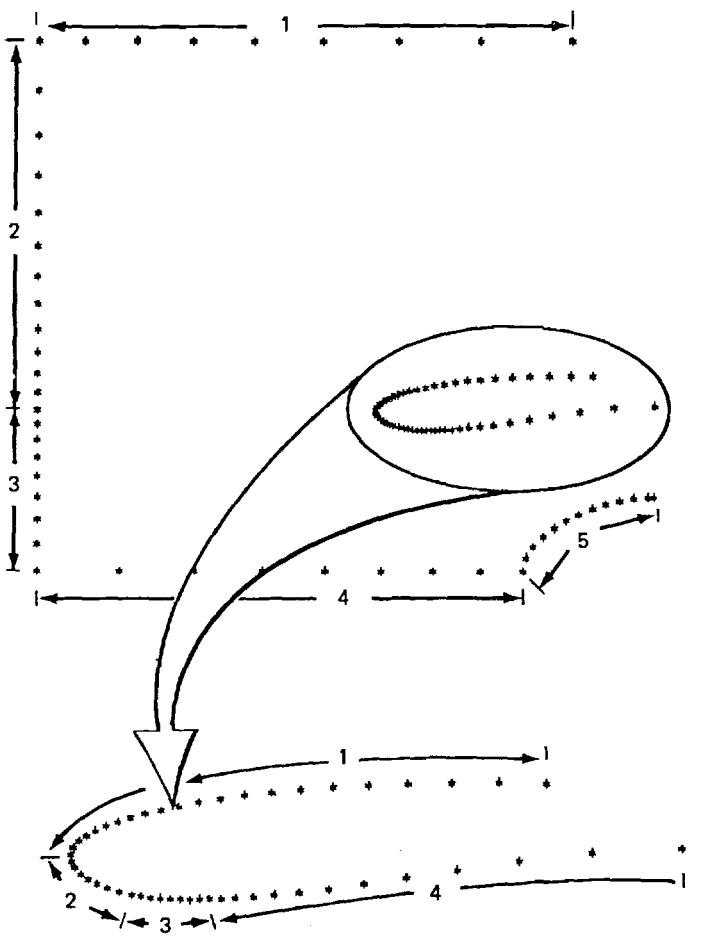

Figure 7.- Geometric progression regions along inlet contour and analysis boundary.

The second extension uses a ramping function to regulate the dependence of the connecting function on the boundary slope. This connecting function is an explicit functional relation used to establish the transformation between the physical domain and the computational domain.

For the mixer lobe, this dependence was regulated to redistribute the internal mesh points and reduce mesh skewness.

In the case of the subsonic inlet, it was found that a constant value for each plane was sufficient to insure against mesh line cross-over.

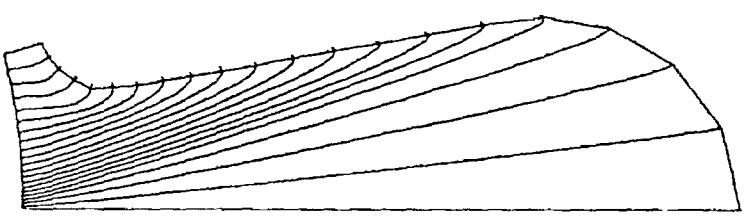

Without ramping function

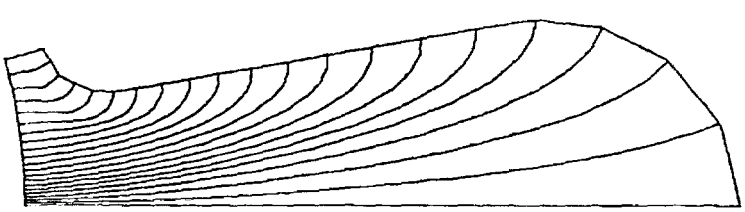

With ramping function

Figure 8.- Connecting function dependency on boundary slope.

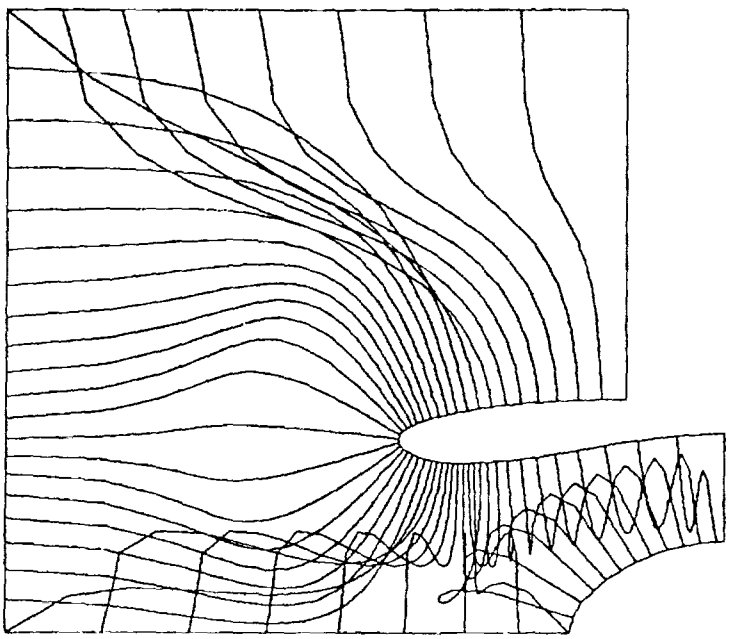

Without ramping function

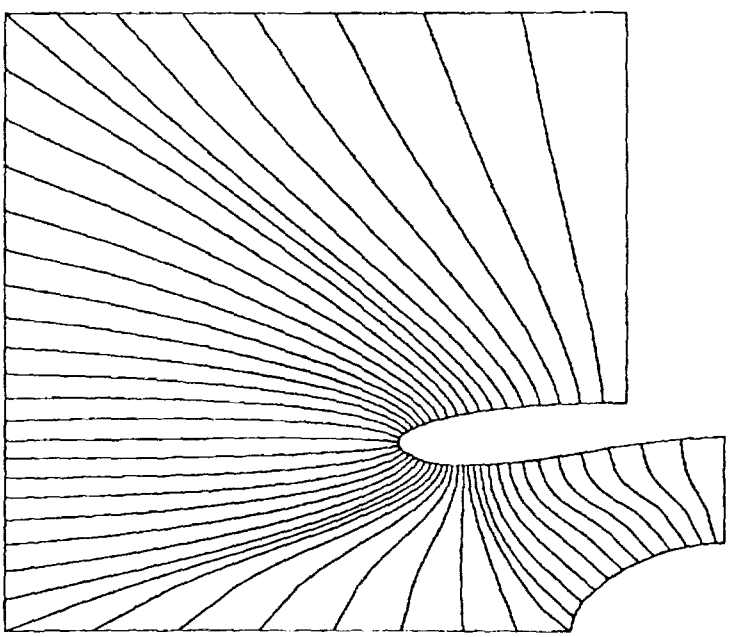

With ramping function

Figure 9.- Connecting function dependency on boundary slope.

The third extension utilizes the concentration function suggested by Smith and Wiegel, but uses it to force the mesh in the direction of both boundaries of the mixer lobe. More mesh was then needed to be linearly added to fill the void created by this mesh concentration.

The inlet only required the mesh to be forced towards the inlet contour. A concentrated mesh was assumed unnecessary along the spinner boundary; it was felt that for a potential flow analysis the flow about the spinner would not propagate upstream and affect the solution at the regions of interest (hilite, throat, etc.). The mesh concentration for both the mixer and the inlet permits flow analysis within the boundary layers.

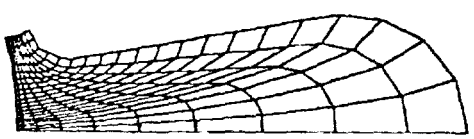

Mesh concentrated towards inner boundary

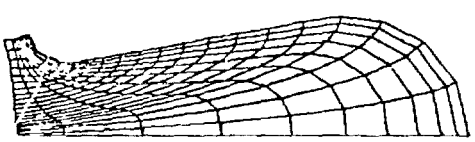

Mesh concentrated towards outer boundary

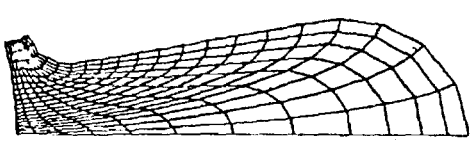

Mesh concentrated towards both boundaries

Figure 10.- Mesh concentration.

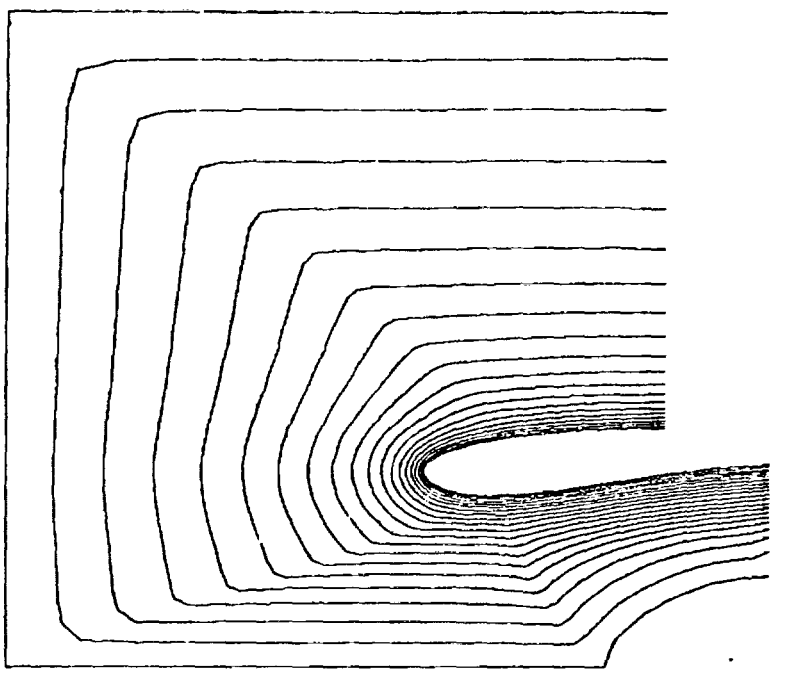

Figure 11.- Mesh concentration.

The fourth extension applies to the subsonic inlet only. It was necessary to produce a computational mesh which possessed a smooth progression of cell metrics and cell volumes in all directions to allow a solution process of a flow analyser to use the grid efficiently. The interior points of the computational mesh were "smoothed" by a multiple application of a five point diffusion operator:

$$X(L,I)_{new} = \alpha \left\{ X(L-1,I) + X(L+1,I) + X(L,I-1) + X(L,I+1) - 4 * X(L,I)_{old} \right\}$$

$$Y(L,I)_{new} = \alpha \left\{ Y(L-1,I) + Y(L+1,I) + Y(L,I+1) + Y(L,I+1) - 4 * Y(L,I)_{old} \right\}$$

The value of α and the number of times of application were determined by trial and error.

The "smoothed" boundary points could not be determined from the five point diffusion operator since one of the required smoothing points would be outside the mesh region. Their values were determined from the intersection of the lines defined by the "smoothed" interior mesh points and the boundaries.

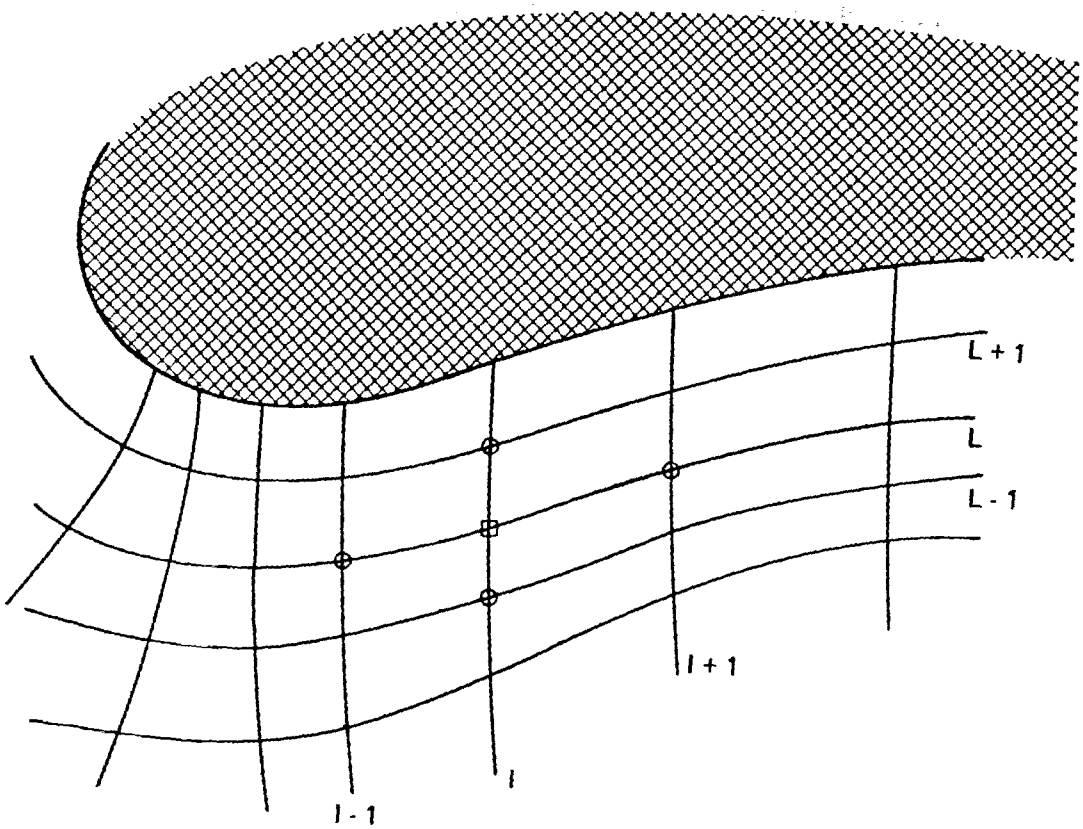

$$X(L,I)_{new} = \alpha \left\{ X(L-1,I) + X(L+1,I) + X(L,I-1) + X(L,I+1) - 4 * X(L,I)_{old} \right\}$$

$$Y(L,I)_{new} = \alpha \left\{ Y(L-1,I) + Y(L+1,I) + Y(L,I+1) + Y(L,I+1) - 4 * Y(L,I)_{old} \right\}$$

Figure 12.- Five point diffusion operator.

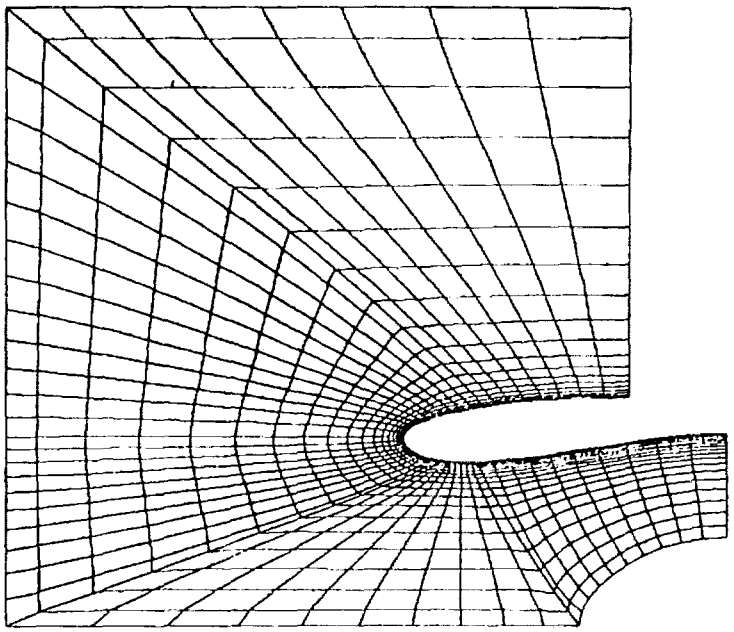

α = 0.05; Number of interations = 1

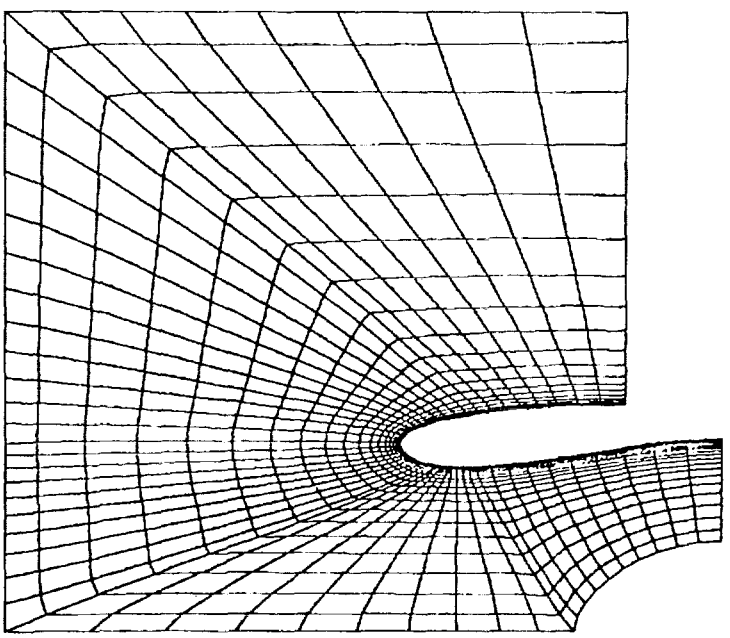

α = 0.05; Number of interations = 3

Figure 13.- "Smoothed" computational mesh.

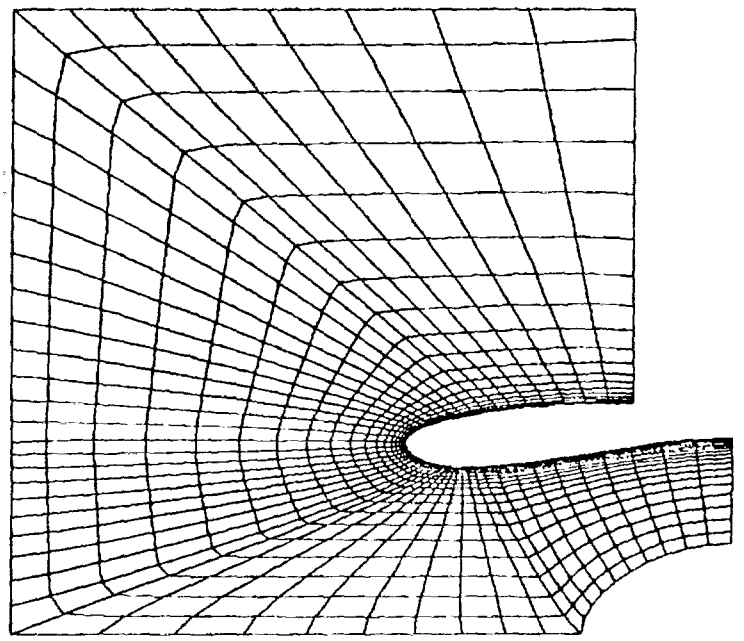

α = 0.05; Number of interations = 6

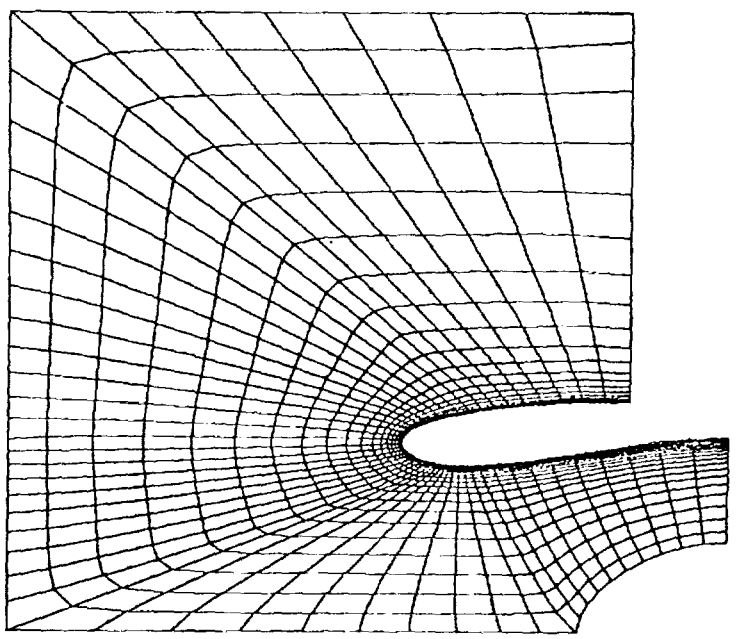

α = 0.05; Number of interations = 12

Figure 13.- Concluded.

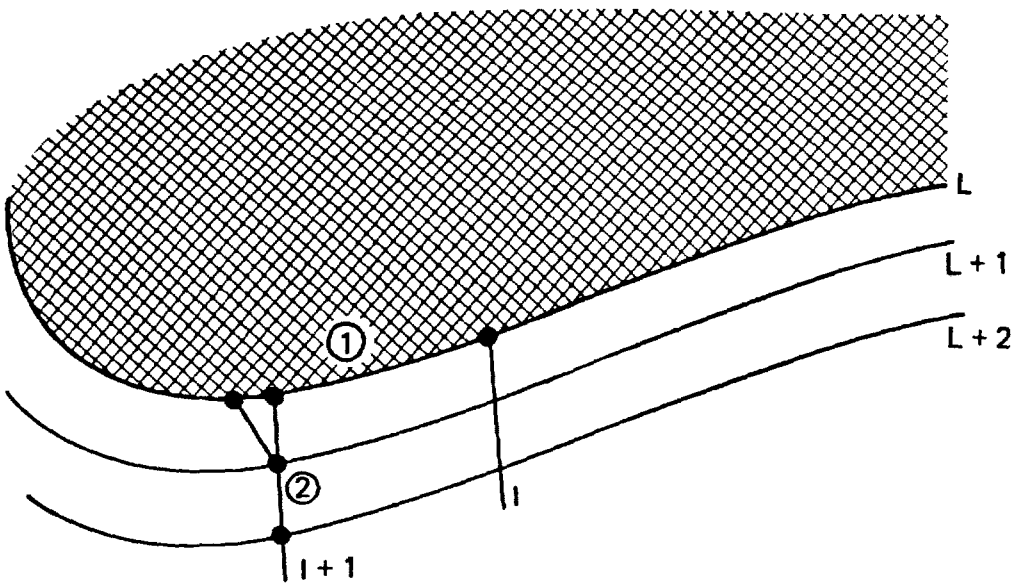

slope of segment ①

$$M_1 = \frac{Y(L, I) - Y(L, I+1)}{X(L, I) - X(L, I+1)}$$

equation of segment ①

$$Y - Y(L,I) = M_1\left\{X - X(L,I)\right\} \qquad ②$$

slope segment ②

$$M_2 = \frac{Y(L+1, I+1) - Y(L+2, I+1)}{X(L+1, I+1) - X(L+2, I+1)}$$

equation of segment ②

$$Y - Y(L+1, I+1) = M_2\left\{X - X(L+1, I+1)\right\} \qquad ①$$

since a line thru segment ② intersects segment ①,
the X's and Y's of equations ① & ② equal each other.
Solving for X:

$$X(L, I+1)_{new} = \frac{M_1\left\{X(L, I)\right\} - M_2\left\{X(L+1, I+1)\right\} + Y(L+1, I+1) - Y(L, I)}{M_1 - M_2}$$

Solving for Y:

$$Y(L, I+1)_{new} = M_1\left\{X(L, I+1)_{new} - X(L, I)\right\} + Y(L, I)$$

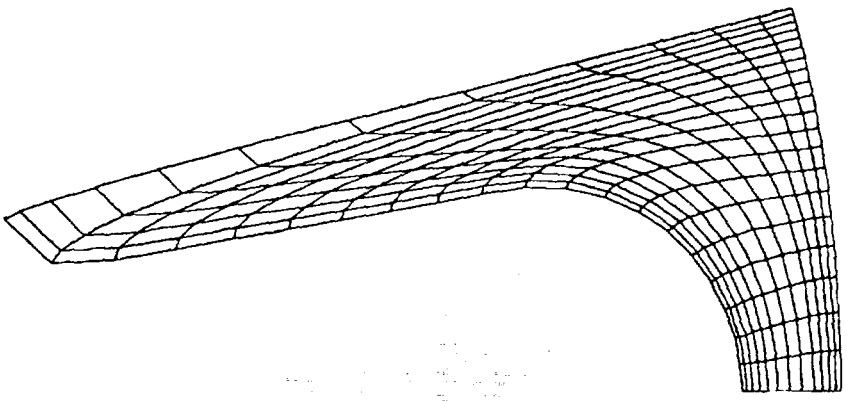

SECONDARY LOBE - PLANE 120
GEOMETRIC PROGRESSION LOWER BOUNDARY 0.9500 UPPER BOUNDARY 1.1000
SLOPE SCALER LOWER BOUNDARY 1.0500 UPPER BOUNDARY 1.1000

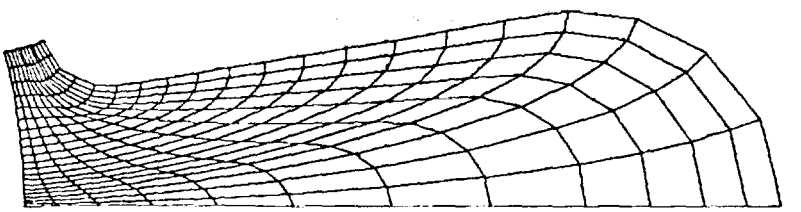

PRIMARY LOBE - PLANE 120
GEOMETRIC PROGRESSION LOWER BOUNDARY 1.1000 UPPER BOUNDARY 1.1000
SLOPE SCALER LOWER BOUNDARY 1.1000 UPPER BOUNDARY 1.1000

Figure 14.- Example mesh for last mixer plane.

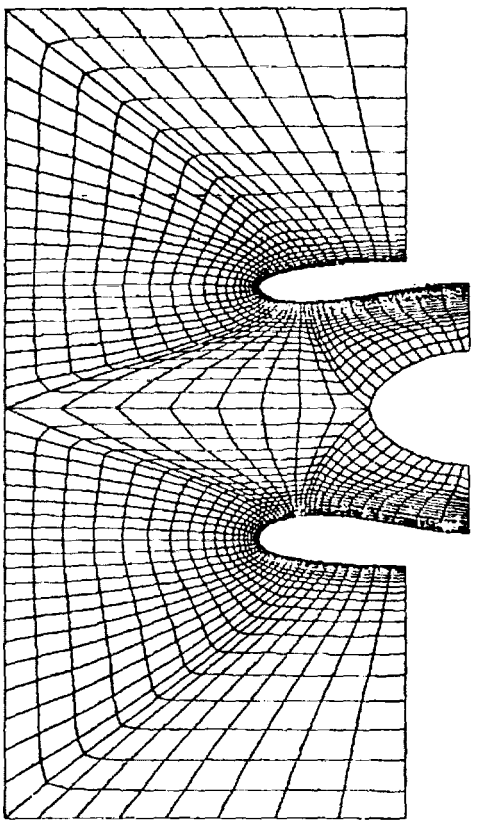

Figure 15.- Example mesh for subsonic inlet.

Conclusions

The method of Smith and Wiegel can be used to generate meshes for mixer lobes and subsonic inlets that are compatible with flow analysis codes requiring a boundary fitted coordinate system. Successful application of this mesh generator required development of procedures to distribute the mesh points along the boundaries, to regulate the dependence of the connecting function to the local boundary slope, to concentrate the mesh into regions of special interest, and to modify the mesh grid so that it possessed a smooth progression of cell metrics and cell volumes in all directions. The method of Smith and Wiegel when coupled with the extensions mentioned above has proven to be easy to use and control for the inlet and mixer lobe geometries investigated.

The next step is the formulation of a truncation error monitor for arbitrary meshes. This monitor will define where in an analysis domain the grid length scales must be changed and by what amount in order to equalize truncation errors over the entire analysis domain. Once these errors have been equalized, this same monitor will use several levels of grid distribution (of the above analysis grid) to then make estimates of the absolute truncation error spectrum. This work is currently under contract with the NASA Langley Research Center.